Journal of Water & Health

IWA PUBLISHING

Journal of Water and Health Vol 21 No 9, 1228 doi: 10.2166/wh.2023.091

Sunlight photolysis of SARS-CoV-2 N1 gene target in the water environment: considerations for the environmental surveillance of wastewater-impacted surface waters

Fiona B. Dunn and Andrea I. Silverman *

Department of Civil and Urban Engineering, Tandon School of Engineering, New York University, Brooklyn, NY 11201, USA
*Corresponding author. E-mail: andrea.silverman@nyu.edu

AIS, 0000-0001-8199-5860

ABSTRACT

Wastewater surveillance of SARS-CoV-2 has been used around the world to supplement clinical testing data for situational awareness of COVID-19 disease trends. Many regions of the world lack centralized wastewater collection and treatment infrastructure, which presents additional considerations for wastewater surveillance of SARS-CoV-2, including environmental decay of the RT-qPCR gene targets used for quantification of SARS-CoV-2 virions. Given the role of sunlight in the environmental decay of RNA, we evaluated sunlight photolysis kinetics of the N1 gene target in heat-inactivated SARS-CoV-2 with a solar simulator under laboratory conditions. Insignificant photolysis of the N1 target was observed in a photosensitizer-free matrix. Conversely, significant decay of the N1 target was observed in wastewater at a shallow depth (<1 cm). Given that sunlight irradiance is affected by several environmental factors, first-order decay rate models were used to evaluate the effect of water column depth, time of the year, and latitude on decay kinetics. Decay rate constants were found to decrease significantly with greater depth of the well-mixed water column, at high latitudes, and in the winter. Therefore, sunlight-mediated decay of the N1 gene target is likely to be minimal, and is unlikely to confound results from wastewater-based epidemiology programs utilizing wastewater-impacted surface waters.

Key words: environmental surveillance, RNA photolysis, SARS-CoV-2, wastewater-based epidemiology

HIGHLIGHTS

- Heat-inactivated SARS-CoV-2 were exposed to simulated sunlight.
- Photolysis rate constants of N1 target in experimental matrices were quantified.
- Significant photolysis of the N1 target was observed in wastewater at shallow depth.
- Decay rate models were used to consider other environmental factors.
- The N1 gene target is likely to persist in sunlit waters due to light attenuation.

GRAPHICAL ABSTRACT

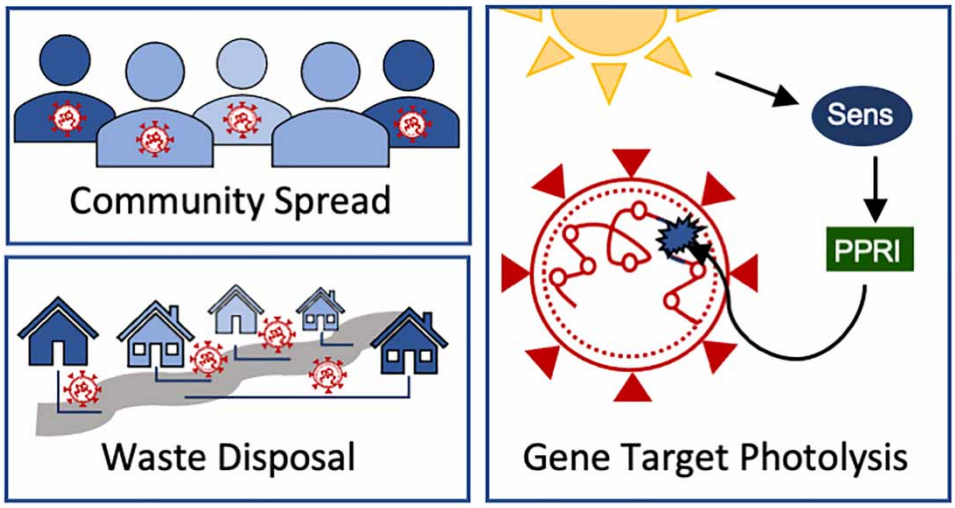

INTRODUCTION

The severe acute respiratory syndrome coronavirus 2 (SARS-CoV-2) is a single-stranded RNA, enveloped virus that causes coronavirus disease 2019 (COVID-19). Symptomatic and asymptomatic COVID-19 patients have been found to shed SARS-CoV-2 RNA in their feces (Tang *et al.* 2020; Park *et al.* 2021), making wastewater-based epidemiology (WBE) a valuable tool for community outbreak surveillance for COVID-19 (Manor *et al.* 1999; Kazama *et al.* 2017). As a result, many global, collaborative efforts have emerged from the COVID-19 pandemic to monitor the presence of SARS-CoV-2 RNA targets in wastewater (Bivins *et al.* 2020; Lundy *et al.* 2021), and wastewater surveillance has been proposed for use in applications that include early detection of SARS-CoV-2 in a sewershed (Randazzo *et al.* 2020), evaluation of public health interventions (e.g., vaccinations, lockdowns, mask mandates) (Hillary *et al.* 2021), identification of sewershed-specific needs for increased testing of COVID-19, and tracking the prevalence of new SARS-CoV-2 variants (Lee *et al.* 2021; Rios *et al.* 2021).

Many wastewater surveillance programs are designed around the presence of centralized sanitation infrastructure, such as piped sewage conveyance systems and community-scale wastewater treatment systems. For example, Hoar *et al.* collected 24-h flow-weighted composite samples of the influent wastewater from New York City's 14 Water Resource Recovery Facilities (WRRFs) once or twice weekly; the samples were analyzed for the SARS-CoV-2 N1 RNA target using RT-qPCR to determine the viral loading rate (N1 gene copies day^{-1}), which was then compared to the 7-day average of new COVID-19 cases per day in each sewershed, as confirmed by clinical testing (Hoar *et al.* 2022). However, many regions around the world lack centralized sanitation infrastructure, and different strategies are needed in the design and implementation of wastewater surveillance programs in communities that are not connected to a sewer network. For example, one recommendation for wastewater surveillance programs in low-income communities not served by a sewer network is to sample the surface waters into which raw sewage is discharged (Calabria de Araujo *et al.* 2020). This approach has been employed previously, for example by Rocha *et al.*, who collected grab samples from the Tijuana River in California, quantified the concentration of SARS-CoV-2 N1 and N2 RNA targets using RT-qPCR, and constructed a model to compare SARS-CoV-2 RNA to the number of COVID-19 cases upstream in Tijuana, Mexico by accounting for the measured flow rate of the river and recorded COVID-19 clinical cases (Rocha *et al.* 2022). When sampling wastewater-contaminated surface waters, however, there are various factors that may present challenges for translating gene target concentrations measured by (RT-)qPCR to estimate trends in disease prevalence in the surrounding community. One such factor is potential decay of the (RT-)qPCR target under surveillance while in the environment.

Sunlight plays an important role in the environmental decay of microbial contaminants (Nelson *et al.* 2018), and nucleic acids (i.e., RNA and DNA) are targets of direct and indirect photolytic mechanisms (Jagger 1985). Direct photolysis occurs when nucleic acids absorb photons of light and become damaged through the formation of photoproducts including

cyclobutane pyrimidine dimers (CPDs), pyrimidine (6-4) pyrimidone adducts (6-4 PP) and their Dewar valence isomers, as well as pyrimidine photohydrates (Görner 1994; Douki & Cadet 2001; Douki 2006). In RNA photolysis, CPDs consist of cytosine and uracil doublets (Miller & Plageman 1974) while pyrimidine photohydrates consist of cytosine and uracil hydrates (Fisher & Johns 1976; Gordon *et al.* 1976; Wurtmann & Wolin 2009). Indirect photolysis occurs when endogenous (i.e., proteins) (Davies & Truscott 2001; Davies 2003) or exogenous photosensitizers (i.e., natural organic matter) absorb light to produce photochemically produced reactive intermediates (PPRI) – including triplet-state dissolved organic matter (^{3}DOM*) and reactive oxygen species (ROS) such as singlet oxygen ($^1O_2$) and hydroxyl radical ($^{\bullet}$OH) – capable of damaging RNA (Cooper *et al.* 1988; Ravanat *et al.* 2001; Nelson *et al.* 2018). $^1O_2$ has been observed to be capable of damaging guanine bases through the formation of photoproducts such as 8-oxo-7 and 8-dihydro-2′-deoxyguanosine (8-oxodGuo) (Ravanat *et al.* 2001). Recently, Zhang *et al.* (2022) found that during simulated sunlight photolysis experiments conducted in the presence of Suwannee River Fulvic Acid (SRFA), ^{3}DOM* had a larger contribution to the decay of extracellular antibiotic resistance genes (ARGs; double-stranded sections of bacterial DNA that encode for resistant traits) than $^1O_2$ and $^{\bullet}$OH, which had small contributions (Zhang *et al.* 2022).

Given the potential for sunlight to degrade RNA targets used for quantifying SARS-CoV-2 in the environment, the goal of this study was to evaluate sunlight-mediated decay of the SARS-CoV-2 N1 gene target, through laboratory experiments and decay rate modeling. While there are several RT-qPCR targets for SARS-CoV-2 (including the N2 RNA target), we selected N1 for this study since it is commonly used for RT-qPCR-based quantification of SARS-CoV-2. Additionally, given the importance of amplicon length (via greater detection of damage on longer amplicons; Dunn & Silverman 2021) and guanine content (via the preferential reaction between PPRI and guanine; Cadet & Teoule 1978) in the photolysis kinetics of RNA targets, and the similar length and guanine content of the N1 (72 bases long; 20.8% guanine content) and N2 targets (67 bases long; 20.9% guanine content), N1 is likely a good proxy for both RNA targets in this context. In addition to collecting data to inform wastewater surveillance program design in locations that lack centralized sewerage, this work provides data related to the sunlight photolysis of viral RNA, more generally.

MATERIALS AND METHODS

Experimental approach

To assess the sunlight-mediated decay of the N1 target, experiments were conducted by exposing heat-inactivated SARS-CoV-2 virions to simulated sunlight for up to 72 h. Experiments were conducted in either photosensitizer-free phosphate-buffered saline (PBS) or a pasteurized wastewater matrix. Details of experiments are as follows.

Simulated sunlight photolysis experiments

A 1600-W solar simulator (Newport #94081A) with an ozone-free Xenon bulb (Newport #62726), an AM0 air mass filter (Newport #81311), and an atmospheric attenuation filter (Newport #71SI00091) to approximate a collimated beam of sunlight was used to conduct sunlight photolysis experiments. Before each experiment, the irradiance spectrum of the solar simulator was measured using a Stellarnet BLK-C spectroradiometer (CR2 cosine receptor). The irradiance spectrum incident on the water surface ($E_{\lambda,0}$; W m^{-2} nm^{-1}; Supplementary Figure S1) was calculated using Supplementary Equation S1, in which the measured solar simulator irradiance with only the AM0 filter installed was corrected for the absorbance of the atmospheric attenuation filter to limit any noise in the UVB region measured by the spectroradiometer. The sums of measured $E_{\lambda,0}$ across the UVB (280–320 nm) and UVA (320–400 nm) regions were 3.3 and 110 W/m^2, respectively. Experimental solution absorbance spectra were measured using a Cary Series UV–Vis spectrophotometer (Agilent Technologies). The solar simulator irradiance spectrum and experimental solution absorbance spectra are provided in Supplementary Figure S1.

Experiments were conducted with heat-inactivated 2019 Novel Coronavirus purchased from the American Type Culture Collection (ATCC VR-1986HK; strain 2019-n-CoV/USA-WA1/2020 isolated from a human case in Washington state). The heat-inactivated 2019 Novel Coronavirus stock solution was diluted approximately 95 times into two separate experimental matrices: (1) sterile, nuclease-free 1X PBS (Invitrogen; 137 mM NaCl, 2.7 mM KCl, 8 mM NaH_2PO_4, 2 mM Na_2HPO_4; pH 7.4) and (2) primary wastewater that was pasteurized and had solids removed, as described below. The initial concentration of the N1 gene target as quantified using RT-qPCR was $(9.09 \pm 1.43) \times 10^4$ copies μL^{-1}. The experimental setup was similar to previous experiments (Dunn & Silverman 2021). Briefly, 250 μL volumes of the experimental solution were aliquoted into sterile 10 mm-diameter polypropylene tubes. The resulting depth of solution was 0.6 cm. The tubes were placed in an

aluminum cooling block in a water bath maintained at 20 °C ± 2 °C and were covered with a 0.125-inch-thick quartz plate (Technical Glass Products). Dark control tubes were covered in aluminum foil to block light transmission. Tubes were collected at set time intervals during the experiment, capped, and stored at 4 °C until RNA extraction, which was performed on the same day as sampling.

To prepare wastewater used as an experimental matrix, primary influent samples from a wastewater treatment plant were collected and pasteurized at 60 °C for 90 min prior to transport on ice to the laboratory. At the laboratory, solids were removed from the samples by centrifugation at 5,000 × *g* for 10 min at 4 °C. The supernatant was transferred to a new sterile tube for storage and the pellet was discarded. Processed wastewater was stored in the dark at 4 °C until use. The dissolved (non-purgeable) organic carbon content of the wastewater was measured to be 14.6 ± 0.25 mg C L^{-1} using a TOC-L_{CSH} Total Organic Carbon Analyzer (Shimadzu) after filtration through a 0.45 μm nylon filter.

RNA extraction and RT-qPCR

After sample collection, 135 μL of each sample was subjected to RNA extraction using the QIAamp Viral RNA Mini Kit (Qiagen). Prior to RNA extraction, 5 μL of purified MS2 stock solution (stock solution concentration = 2.36×10^9 PFU mL^{-1}) was added to the 135 μL subsample, to serve as an extraction control; the mean *Cq* value of the MS2 RT-qPCR assay across experiments was 16.48 ± 0.45. All MS2 spikes were from the same stock solution to ensure that a consistent concentration was added to each sample; details of MS2 propagation and purification were described previously (Silverman *et al.* 2019). Extracted RNA was aliquoted into smaller volumes and stored at −80 °C.

RT-qPCR was conducted on all samples using two assays: the SARS-CoV-2 N1 assay to quantify decay of the gene target (Lu *et al.* 2020), and an MS2 assay targeting the replicase ß chain gene to assess RNA extraction efficiency (Williams 2009). Primer and probe sequences are provided in Supplementary Table S1. RT-qPCR assays were conducted using a QuantStudio 3 real-time PCR system (Applied Biosystems). The thermocycling conditions were as follows: 25 °C for 2 min, 50 °C for 15 min, 95 °C for 2 min, followed by 45 cycles of 95 °C for 3 s, and the target-specific annealing temperature (Supplementary Table S1) for 30 s. Each 20 μL RT-qPCR reaction contained 1X TaqPath 1-Step RT-qPCR Master Mix, CG (Applied Biosystems), the appropriate concentration of primers and probes (Supplementary Table S1), either 5 or 6 μL of template for SARS-CoV-2 or MS2 assays, respectively, and nuclease-free water for dilution to the total volume. All samples were analyzed in triplicate RT-qPCR reactions. Standard curves were included on every RT-qPCR plate and consisted of serial dilutions of the 2019-nCOV_N positive control plasmid (Integrated DNA Technologies) for the N1 assay and extracted RNA from purified MS2 for the MS2 assay. The mean amplification efficiency and R^2 values of RT-qPCR standard curves, presented with their standard deviations, were 104% ± 4.1% [$R^2 = (0.990 \pm 0.004)$] and 99.8% ± 1.02% [$R^2 = (0.996 \pm 0.006)$] for the N1 and MS2 assays, respectively.

Calculation of first-order decay rate constant (k_{obs}^{N1})

We previously derived a relative qPCR quantification method for calculation of DNA decay kinetics, using a modified Δ*Cq* approach that considers the qPCR reaction efficiency (Dunn & Silverman 2021). A similar approach was used here with an additional normalization factor to account for potential differences in RNA extraction efficiency across samples to confirm that any measured differences in N1 concentration (relative to the $t = 0$ sample) are due to sunlight decay and not variations in extraction efficiency. Given that a relative quantification approach was used and the possibility that the *Cq* value of samples with the same target concentration may vary across different qPCR plates due to variations in amplification efficiency, all sample time points from a replicate experiment were run on the same RT-qPCR plate for each RT-qPCR assay (N1 and MS2).

As described above, immediately prior to RNA extraction, all subsamples were spiked with the same amount of MS2. Therefore, any differences in the measured quantification cycle (*Cq*) of the MS2 assay between samples can be attributed to variation in RNA extraction efficiency. We, therefore, used the differences in *Cq* values measured by the MS2 assay to account for differences in extraction efficiency of all RNA in the sample (including the N1 gene target). As such, Equation (1) was used to determine the first-order observed decay rate constant of the N1 gene target (k_{obs}^{N1}), accounting for (i) the amplification factor ($Amp_{F,x}$), which is a function of the amplification efficiency, *m* (Equation (2)), of the RT-qPCR assay (*x*) and (ii) the N1 and MS2 RT-qPCR quantification cycles for samples collected at $t = 0$ (Cq_0) and time *t* (Cq_t). The derivation of

Equation (1) is provided in Supplementary Equations S2–S9:

$$k_{obs}^{N1} \cdot t = -(ln(Amp_{F,\,N1}^{Cq_0^{N1}-Cq_t^{N1}}) + ln(Amp_{F,MS2}^{Cq_t^{MS2}-Cq_0^{MS2}})) \quad (1)$$

$$\mathrm{Amp}_{F,x} = 10^{-1/m} \quad (2)$$

To determine $k_{\mathrm{obs}}^{\mathrm{N1}}$, replicate $-(\ln(\mathrm{Amp}_{F,\,\mathrm{N1}}^{Cq_0^{\mathrm{N1}}-Cq_t^{\mathrm{N1}}}) + \ln(\mathrm{Amp}_{F,\mathrm{MS2}}^{Cq_t^{\mathrm{MS2}}-Cq_0^{\mathrm{MS2}}}))$ values for each time point were pooled and plotted versus time (t); $k_{\mathrm{obs}}^{\mathrm{N1}}$ were calculated as the slope of the best-fit line, determined by linear regression.

Determination of steady-state PPRI concentrations and normalized rate constants

Bulk-phase, steady-state singlet oxygen concentrations ($[\,^1O_2\,]_{ss,exp}$) were determined for wastewater samples through photolysis experiments using furfuryl alcohol (FFA) as a probe compound. Steady-state triplet-state DOM ($[\,^3DOM^*]_{ss,exp}$) concentrations were determined for the wastewater samples using 2,4,6-trimethylphenol (TMP) as a probe compound. A stock solution of FFA (Acros; 98% purity) was prepared in HPLC-grade acetonitrile at a concentration of 11 mM on the day of the experiment. A stock solution of TMP (Alfa Aesar; 98%) was added to 98% Milli-Q water and 2% HPLC-grade acetonitrile to a concentration of 5 mM prior to the experiment and stored in the dark at 4 °C. To assess decay of the probe compounds during photolysis experiments, an initial concentration of either 40 μM FFA or 10 μM TMP was added to 22 mL of the wastewater sample used as an experimental matrix (the wastewater was pre-filtered through a 0.2 μm nylon filter), in 250 mL beakers. The beakers were painted black and mixed with magnetic stir bars. The depth of solution was the same across all laboratory experiments in this study (0.6 cm). Around 180 μL samples were collected intermittently over the course of a 6-h experiment and analyzed by a 1260 Infinity II HPLC (Agilent) with an InfinityLab Poroshell HPH-C18 3.0 × 150 mm 4 μm column (Agilent) fitted with an InfiinityLab Poroshell EC-C18 3.0 × 5 mm 2.7 μm guard column and eluted with Milli-Q water and 10% acetonitrile and analyzed at a wavelength of 219 nm for FFA or 220 nm for TMP. Dark experiments were maintained in the same way except that they were covered with aluminum foil. Experiments were conducted in duplicate. Methodology for the calculation of ($[\,^1O_2\,]_{ss,\,exp}$) and ($[\,^3DOM^*]_{ss,\,exp}$) is included in Supplementary Equations S10 and S11. Briefly, decay of probe compounds was monitored as described above to determine the first-order observed decay rate constants of each probe, $k_{\mathrm{obs,probe}}$ (h^{-1}). $k_{\mathrm{obs,probe}}$ values were then translated into the steady-state PPRI concentrations based on the known second-order reaction rate constants between each PPRI and their respective probes. $k_{q,\mathrm{FFA},\,^1O_2}$ is the second-order rate constant for reaction between FFA and $^1O_2$, and was previously reported to be 1.00×10^8 $M^{-1}\,s^{-1}$ at 22 °C (Appiani *et al.* 2017). In this study, $k_{q,\mathrm{FFA},\,^1O_2}$ was adjusted to 20 °C (the temperature used for experiments) and was determined to be 0.6×10^8 $M^{-1}\,s^{-1}$. Erickson *et al.* previously determined the average second-order reaction rate constant between TMP and ^{3}DOM* ($k_{q,\mathrm{TMP},\,^3DOM^*}$) from different DOM isolates and water samples to be 8.1×10^8 $M^{-1}\,s^{-1}$ (Erickson *et al.* 2018).

The wastewater matrix was filtered prior to experiments conducted to determine PPRI concentrations to aid with HPLC measurements, but not prior to sunlight experiments with SARS-CoV-2. Nevertheless, we believe that a large portion of particulate organic matter (POM) was already removed during the centrifugation step used to prepare wastewater for the SARS-CoV-2 experiments. Additionally, we do not believe that filtration would significantly change the measured steady-state $^1O_2$ concentration given findings by Appiani and McNeil, who determined that probe compounds with a low logK_{oc} (i.e., organic carbon partition coefficient), including FFA, only significantly react with $^1O_2$ in the aqueous phase. Therefore, removal of POM would not greatly affect the amount of $^1O_2$ measured in bulk solution, especially when POM accounts for only a small amount of total organic matter in the sample (Appiani & McNeill 2015).

Prediction of t_{90} in the environment

To extrapolate $k_{\mathrm{obs}}^{\mathrm{N1}}$ measured in the laboratory in a shallow solution (consistent with near-surface conditions) to deeper water columns and a range of incident sunlight spectra, we modeled the time to reach 90% removal of the N1 gene target ($t_{90}^{l,i,j}$; h), in a well-mixed water column with depth l at latitude i and time of year j using Equation (3). Given that endogenous photolysis of the N1 gene target was found to be insignificant and exogenous decay mechanisms dominated (as detailed in the Results and Discussion section), we modeled $t_{90}^{l,i,j}$ based on exogenous photolysis alone. Additionally, given that wastewater generates a heterogeneous mixture of PPRI that contribute to $k_{\mathrm{obs}}^{\mathrm{N1}}$ and that further work is required to determine the individual contributions of each PPRI in diverse environmental matrices, we chose use $^1O_2$ as a proxy for modeling overall indirect photolysis

rates, and therefore calculated $t_{90}^{l,i,j}$ as a function of the decay rate constant of the N1 gene target normalized by $[\,^1O_2\,]_{ss,\,exp}$ ($k^{N1}_{norm,[\,^1O_2\,]_{ss}}$; $M^{-1}\,s^{-1}$; Equation (4)). The average steady-state singlet oxygen concentration over water depth l at latitude i and time of year j, ($[\,^1O_2]^{l,i,j}_{ss}$; M) was predicted using a previously published model by Partanen *et al.* (2021; Equations (5) and (6)):

$$t_{90}^{l,i,j} = \frac{-\ln 0.1}{k^{N1}_{norm,[\,^1O_2\,]_{ss}} \cdot [\,^1O_2]^{l,i,j}_{ss}} \tag{3}$$

$$k^{N1}_{norm,[\,^1O_2\,]_{ss}} = \frac{k^{N1}_{obs,ww}}{[\,^1O_2\,]_{ss,\,exp}} \tag{4}$$

$$[\,^1O_2]^{l,i,j}_{ss} = \frac{R^{l,i,j}_{f,\,^1O_2}}{k_d} \tag{5}$$

$$R^{l,i,j}_{f,\,^1O_2} = \sum_{\lambda} \frac{I^{i,j}_{0,\lambda}}{l} \cdot (1 - e^{-K_{d,\lambda} l}) \cdot (1 - f_{backscatter}) \cdot f_{abs,CDOM} \cdot \Phi_{\Delta,\lambda} \cdot \Delta\lambda \tag{6}$$

In Equations (5) and (6), $R^{l,i,j}_{f,\,^1O_2}$ is the average rate of formation of $^1O_2$ across water depth l (summed over the wavelengths of 280–550 nm to fully capture light absorbance by dissolved organic matter; $M\,s^{-1}$), k_d is the deactivation rate constant for $^1O_2$ in water [$(2.76 \pm 0.02) \times 10^5\ s^{-1}$ (Appiani *et al.* 2017)], $I^{i,j}_{0,\lambda}$ is the irradiance incident on the top of the water column (mmol photons $cm^{-2}\,s^{-1}\,nm^{-1}$; further described below), l is the well-mixed water depth ($l = 1$ cm for near-surface conditions), $K_{d,\lambda}$ is the diffuse attenuation coefficient (Equation (7); cm^{-1}), $f_{backscatter}$ is the fraction of light that is backscattered out to the water column, $f_{abs,CDOM}$ is the fraction of the total absorbance that is attributed to absorbance by chromophoric dissolved organic matter (CDOM), and $\Phi_{\Delta,\lambda}$ is the wavelength-dependent $^1O_2$ quantum yield (described below). The values input for $f_{backscatter}$ (0.03) and $f_{abs,CDOM}$ (0.7) were taken from the representative case presented by Partanen *et al.* (2021).

$I^{i,j}_{0,\lambda}$ values were calculated as day-averaged irradiance values for the solar equinoxes (approximated as June 21st and December 22nd when solar declination is equal to 0°) and solar solstices (approximated as March 20th and September 22nd when solar declination is equal to $\pm$ 23.4°) at several latitudes in the northern and southern hemispheres from published solar irradiance reference spectra (Apell & McNeill 2019), which were modeled by the simple model of the atmospheric radiative transfer of sunshine (SMARTS; global horizontal irradiance (Gueymard 2005)).

$K_{d,\lambda}$ was modeled using the dissolved organic carbon (DOC) concentration of the wastewater used in experiments (14.59 mg C L^{-1}; Equation (7)) (Partanen *et al.* 2021):

$$K_{d,\lambda} = \exp(-0.01347\lambda + 5.36(DOC)^{0.157}) \tag{7}$$

$\Phi_{\Delta,\lambda}$ was modeled using the average case of a biexponential wavelength-dependent model published by Partanen *et al.* (2021), which was developed using experimental data in which Φ_Δ was measured using different sources of CDOM including Étang de la Gruère water, Pony Lake Fulvic Acid (PLFA), Suwannee River NOM, and Suwannee River water as described by Partanen *et al.* (2020, 2021). Of note is that the $\Phi_{\Delta,\lambda}$ values used to develop the model represent data from microbially derived CDOM (PLFA), terrestrially derived CDOM (SRNOM), and whole water samples (from Étang de la Gruère and Suwannee River), which may differ from those of wastewaters and wastewater-impacted surface waters given their greater presence of wastewater organic matter. We also assume that $\Phi_{\Delta,\lambda}$ and $k^{N1}_{norm,[\,^1O_2\,]_{ss}}$ are the same for each latitude and season evaluated.

To evaluate the impact of light attenuation in the water column on observed decay rates of the N1 gene target, we modeled $t_{90}^{l,i,j}$ at near-surface conditions and over well-mixed water depths up to 50 cm using Equations (4)–(6).

Statistical analysis

Statistical analyses were conducted in GraphPad Prism 9.3.1. To determine if first-order reaction rate constants were significantly different from each other, two-tailed hypothesis tests were used to test the null hypothesis that slopes of best-fit linear regressions were the same. *P*-values were computed at 95% confidence intervals, in which *P*-values less than 0.05 indicate significant differences. All rate constants are presented with the standard error, unless indicated otherwise.

RESULTS AND DISCUSSION

Photolysis experiments in PBS

Two replicate experiments were conducted with heat-inactivated SARS-CoV-2 inoculated in PBS; duplicate samples were collected at each time point during each experiment. We consistently measured a large initial decrease (average = 1.6-log) in the N1 gene target concentration between the unexposed sample and the first sample collected after exposure to simulated sunlight (i.e., between the $t = 0$ and $t = 4$ h samples), after which there was minimal decay of the N1 target over the course of the 72-h experiment. Given no observed decay of the N1 target over 68 h, it is unlikely that the cause of the initial observed decrease in N1 concentration was due to sunlight exposure. It is unknown why there was an observed 1.6-log decrease in the N1 concentration within the first 4 h of the experiment, but some possibilities include adsorption of virus particles to the inner surface of the polypropylene tubes (Richter *et al.* 2021) or a higher susceptibility of a subset of the SARS-CoV-2 RNA to degradation. We, therefore, calculated the first-order observed decay rate constant of the N1 gene target in PBS ($k^{N1}_{obs,PBS}$) as the slope of the linear regression line for time points >0 h (i.e., we did not include the $t = 0$ time point in the linear regression; Figure 1(a)). The resulting $k^{N1}_{obs,PBS}$ was not found to be significantly different from zero [$P = 0.20$; $k^{N1}_{obs,PBS} = (3.40 \pm 2.60) \times 10^{-3}\ h^{-1}$; $R^2 = 0.08$]. Similarly, the dark decay rate constant of the N1 gene target for $t \geq 4$ h was not found to be significantly different from zero [$P = 0.08$; $k^{N1}_{obs,PBS,dark} = (1.52 \pm 0.76) \times 10^{-2}\ h^{-1}$; $R^2 = 0.37$].

Given that experiments conducted in PBS did not contain PPRI-producing exogenous photosensitizers, we assume that only endogenous photolysis occurred in this solution. Our finding that there was minimal direct photolysis of the short, 72-base N1 gene target is in line with Qiao & Wigginton (2016), who studied the kinetics of sunlight-mediated decay of two RNA oligomers from the MS2 genome (both 24 bases in length) and observed no significant decay of either oligomers after 5 h of simulated sunlight irradiation (with decay measured using RT-qPCR), although these previous experiments were much shorter than those conducted herein. We previously conducted 72-h long simulated sunlight experiments to quantify the photolysis rate constants of extracellular and intracellular ARGs (regions of bacterial, double-stranded DNA which encode resistance to antibiotics) in PBS, and also found insignificant decay of short-amplicon (~100 base pair) qPCR targets (Dunn & Silverman 2021).

The insignificant direct photolysis rate observed for the RT-qPCR target is not necessarily indicative of decay of longer gene targets or of photoinactivation of the virus itself. For example, we expect that greater direct photolysis rate constants would be measured if an RT-qPCR assay with a longer gene target was employed, given more potential photodamage sites available (Ho *et al.* 2016; Dunn & Silverman 2021). Additionally, coronaviruses are hypothesized to have some of the fastest rates of photoinactivation among viruses (Sagripanti & Lytle 2020), given that they have the largest genomes of the ssRNA viruses (29–31 kb). While the RT-qPCR assay used to quantify decay rates herein does not reflect the impact of sunlight photolysis on virus inactivation, it was chosen to assess the environmental stability of the N1 gene target with sunlight exposure, due to its direct relevance to WBE applications.

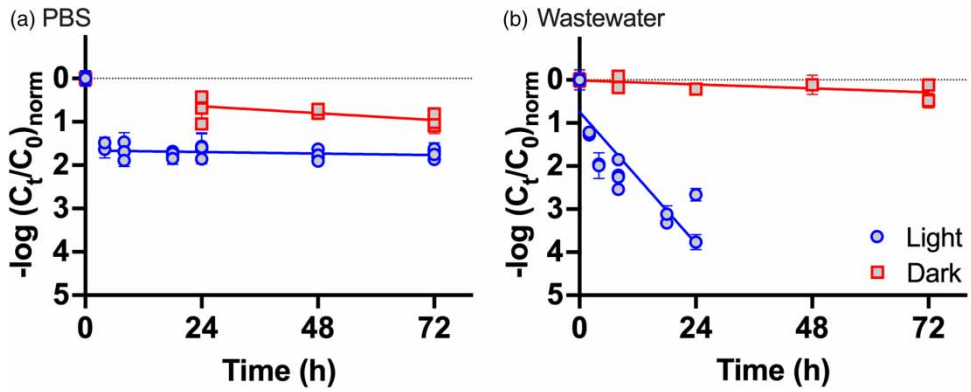

Figure 1 | Simulated sunlight photolysis of N1 gene target from heat-inactivated SARS-CoV-2 in (a) PBS and (b) wastewater, under simulated sunlight and dark control conditions. The concentration of N1 was quantified using RT-qPCR and normalized for potential differences in extraction efficiency using bacteriophage MS2 as an extraction control. Each point represents individual replicate measurements from four experiments started on two separate days. Best-fit linear regression lines are plotted as solid lines for $t > 0$ in panel (a) and $t \geq 0$ in panel (b). Error bars represent the standard deviation of triplicate RT-qPCR reactions for each data point; some error bars are smaller than the symbols.

Photolysis experiments in a wastewater matrix

In contrast to experiments conducted in PBS, a large initial decrease in N1 concentration was not measured in experiments conducted in the dark in pasteurized wastewater. One possibility for this observation is that wastewater constituents may have coated the inner surface of the polypropylene tubes used as experimental reactors, therefore preventing the adsorption of virus particles and apparent decrease in N1 target concentrations. Given this observation in dark samples, we assume all decay of the N1 target in wastewater in light-exposed samples was due to sunlight-mediated processes.

The first-order observed sunlight-mediated decay rate constant of the N1 gene target in pasteurized wastewater ($k^{N1}_{obs,ww}$), measured using RT-qPCR, was $(2.93 \pm 0.45) \times 10^{-1}\,h^{-1}$ ($R^2 = 0.75$), which was calculated including data from samples collected at $t \geq 0$ (Figure 1(b)). Twenty-four hours of simulated sunlight exposure resulted in almost 4-log decay of the N1 gene target, after which the concentration was below the limit of detection for the N1 RT-qPCR assay (20 copies μL^{-1}); the limit of detection was determined as the concentration of the most diluted standard for which at least 95% of the replicate reactions were able to be quantified by RT-qPCR (Forootan *et al.* 2017). Given minimal endogenous inactivation measured during experiments in PBS, it is assumed that sunlight-mediated decay in wastewater is caused by exogenously produced PPRI.

Due to safety requirements of working with SARS-CoV-2 virions in the laboratory, experiments were conducted with a heat-inactivated standard stock solution of the virus (the pasteurization conditions were noted to be 65 °C for 30 min by ATCC, the supplier). It is unknown if the process of heat inactivation changed the physicochemical properties of the virus in a way that could influence the sunlight-mediated decay kinetics of the RNA target assessed in this paper. Previous research evaluating the impact of heat applied to enveloped viruses, including pasteurization and dry heat treatments, observed disruption of the lipid envelope, denaturation of proteins within the capsid, and exposure of the capsid proteins to subsequent damage from proteolytic enzymes (Aloia *et al.* 1988; Pfaender *et al.* 2015; Gröner *et al.* 2018). Wigginton *et al.* evaluated the influence of heat inactivation, among other disinfectants, on several physical and chemical properties of the non-enveloped bacteriophage MS2, and attributed loss of MS2 infectivity under heat treatment to a disruption to the bacteriophage's ability to bind to the host cell; damage to the MS2 genome from heat treatment was determined to be negligible (Wigginton *et al.* 2012). However, despite previous research finding minimal decay of viral nucleic acids due to heat inactivation, it remains unclear whether heat-mediated damage to other macromolecules could make SARS-CoV-2 RNA more susceptible to exogenously produced PPRI.

The dark decay rate constant of the N1 gene target in wastewater [$k^{N1}_{obs,ww,dark} = (8.85 \pm 3.15) \times 10^{-3}\,h^{-1}$; $R^2 = 0.50$] was statistically different from zero ($P < 0.05$), however, it was very small and significantly lower than $k^{N1}_{obs,ww}$ ($P < 0.0001$). We observed an average of 0.3-log decay of the N1 gene target in the pasteurized wastewater matrix under dark conditions over the course of the 72-h experiments; the corresponding t_{90} was approximately 10.8 d. This finding is similar to that of Ahmed *et al.*, who determined t_{90} of the N1 gene target (in gamma-irradiated SARS-CoV-2), determined by RT-qPCR, to be 20.4 ± 2.13 d and 29.9 ± 2.39 d in untreated and autoclaved wastewater, respectively, at 15 °C under dark conditions (Ahmed *et al.* 2020).

The bulk-phase, steady-state singlet oxygen concentration ($[^1O_2]_{ss,exp}$) in wastewater was determined to be $(2.32 \pm 0.06) \times 10^{-13}$ M. The steady-state triplet-state DOM concentration ($[^3DOM^*]_{ss,exp}$) was determined to be $(8.06 \pm 1.10) \times 10^{-14}$ M. The decay of FFA and TMP in dark experiments in wastewater was not significantly different from zero ($P = 0.67$ and 0.05, respectively), indicating that there was no PPRI formation in the dark.

In the Qiao and Wigginton study discussed above, simulated sunlight irradiation of an experimental matrix containing Rose Bengal, a $^1O_2$ photosensitizer, resulted in significant decay of two RNA oligomers from the MS2 genome, as measured using RT-qPCR (Qiao & Wigginton 2016). The second-order reaction rate constants for indirect photolysis by $^1O_2$ (from experiments with a steady-state $^1O_2$ concentration of 9.0×10^{-11} M) were calculated to be $(1.1 \pm 0.14) \times 10^6$ $M^{-1}s^{-1}$ and $(6.5 \pm 0.33) \times 10^6\,M^{-1}s^{-1}$ for Oligomers A and B, respectively; Oligomer B had a greater guanine content than Oligomer A (Qiao & Wigginton 2016). In the present study, when $k^{N1}_{obs,ww}$ was normalized by measured $[^1O_2]_{ss,exp}$ (Equation (3)), the resulting $k^{N1}_{norm,[^1O_2]_{ss}}$ was equal to $3.51 \times 10^8\,M^{-1}s^{-1}$, which was several orders of magnitude higher than the second-order reaction rate constants of the RNA oligomers with $^1O_2$ determined by Qiao and Wigginton. This finding is likely due to the contribution of additional PPRI, such as $^3DOM^*$, to exogenous inactivation, given that wastewater contains a heterogeneous mixture of photosensitizers that produce a range of PPRI. Additionally, decay rate constants could be enhanced due to possible associations between the SARS-CoV-2 virion with DOM present in the wastewater matrix used in experiments. As discussed above, Zhang *et al.* (2022) found that $^3DOM^*$ contributed the most to decay of extracellular ARGs

during simulated sunlight experiments, and the contributions of $^1O_2$ and $^{\bullet}OH$ were small (Zhang *et al.* 2022). However, during sunlight photolysis experiments conducted in Suwannee River Dissolved Organic Matter (SRDOM), Zhang *et al.* (2019) determined that ^{3}DOM* did not contribute significantly to extracellular ARG decay (Zhang *et al.* 2019). The findings of these studies illustrate that more work is needed to better understand the contributions of different PPRI to DNA and RNA photolysis.

Understanding decay at different latitudes, times of the year, and over well-mixed depth

To understand how sunlight-mediated decay rates are impacted by diurnal and seasonal variation in sunlight intensity and geographic location, we used the decay rate constants measured during laboratory experiments to model times required to reach 90% decay ($t_{90}^{l,i,j}$) of the N1 gene target at different latitudes (i) (i.e., 0°, 20°, and 40° in the northern and southern hemispheres) at different times of the year (j) over well-mixed depths l including near-surface ($l = 1$ cm) and greater depths up to 50 cm.

Given that endogenous sunlight decay of the N1 gene target was found to be minimal, and exogenous decay was found to be significant in the presence of photosensitizers in wastewater, the inactivation rate model focused on the exogenous inactivation mechanism alone. Although it is unclear from current work which PPRI is most important for RNA decay, we chose to model decay of the N1 target in terms of $[\,^1O_2]_{ss}$ – under the assumption that $^1O_2$ can be used as a proxy for estimating PPRI-mediated indirect photolysis as a whole – given (i) the observed involvement of $^1O_2$ in the photolysis of RNA (Qiao & Wigginton 2016), (ii) that ^{3}DOM* is a precursor for $^1O_2$ (Latch & McNeill 2006), and (iii) the availability of models to approximate $[\,^1O_2]_{ss}$ in environmental waters with different sunlight irradiance. More specifically, we used $k^{N1}_{norm,[\,^1O_2\,]_{ss}}$, the observed decay rate constant of the N1 gene target in wastewater normalized by $[\,^1O_2]_{ss,\,exp}$, along with modeled average steady-state singlet oxygen concentration ($[\,^1O_2]_{ss}^{l,i,j}$) to account for different incident light (due to different latitudes or times of the year) and light attenuation in a well-mixed water column.

Modeled near-surface $t_{90}^{l=1,i,j}$ values are displayed in Figure 2. Near-surface $t_{90}^{l=1,i,j}$ values were calculated over a depth of 1 cm (representing the top of the water column). Since near-surface $t_{90}^{l=1,i,j}$ values are not impacted by light attenuation, they are likely not representative of sunlight decay in most environmental waters. Seasonal variation largely does not impact near-surface $t_{90}^{l=1,i,j}$

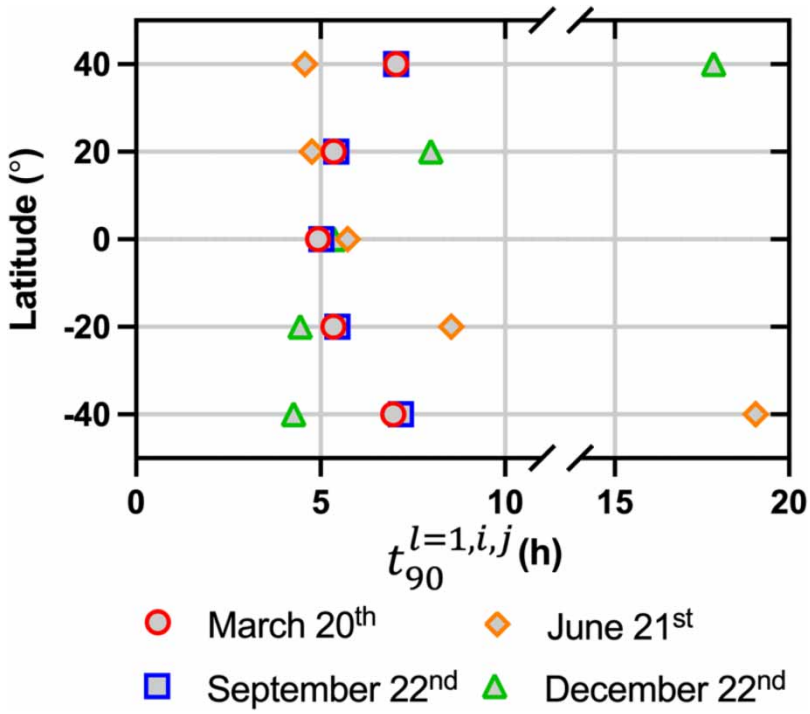

Figure 2 | Predicted times required to reach 90% decay ($t_{90}^{l=1,i,j}$) of the SARS-CoV-2 N1 gene target at different latitudes and times of the year at near-surface conditions $l = 1$ cm. These data are also presented in Supplementary Figure S3, with individual data sets presented in separate panels.

values at the equator. However, the impact of seasonal variation on near-surface $t_{90}^{l=1,i,j}$ values increases further away from the Equator due to seasonal changes in incident light intensity. For example, at the Equator, modeled near-surface $t_{90}^{l=1,i,j}$ values range from 4.9 to 5.7 h over the course of the year, whereas at 40°S, near-surface $t_{90}^{l=1,i,j}$ values range from 4.3 to 19 h.

In wastewater and environmental waters, light intensity within the water column decreases exponentially as a function of depth according to Beer's Law, thereby decreasing the amount of light available for photochemical reactions, including production of PPRI. Therefore, production of PPRI decreases with water depth, and most sunlight-mediated reactions occur close to the water surface. For example, Partanen *et al.* found that although the DOC concentration contributes most to determining near-surface $[^1O_2]_{ss}$, the depth of the epilimnion is the largest contributing environmental factor influencing depth-averaged $[^1O_2]_{ss}$ over the epilimnion of a lake (Partanen *et al.* 2021). Given these considerations, we also modeled $t_{90}^{l,i,j}$ over a well-mixed depth (l) up to 50 cm.

Figure 3(a) presents the $t_{90}^{l,i,j}$ modeled over different depths using the representative cases of June 21st and December 22nd at 40°S (i.e., the conditions representing the maximum and minimum modeled near-surface $t_{90}^{l=1,i,j}$, respectively). In these representative cases, the $t_{90}^{l,i,j}$ for N1 target decay in well-mixed water depths of 20 cm were estimated to be 8.9 and 2.1 d for June 21st and December 22nd at 40°S, respectively. These $t_{90}^{l,i,j}$ values were even greater over deeper well-mixed depths, indicating that the N1 gene target is likely to be minimally impacted by sunlight-mediated processes over depths representative of environmental waters. While modeled near-surface $t_{90}^{l=1,i,j}$ values are relatively small (on the order of hours), when modeling over greater well-mixed depths more representative of environmental water bodies, $t_{90}^{l,i,j}$ values quickly increase (to the order of days).

More generally, when calculating the ratio of $t_{90}^{l,i,j}$ at well-mixed depths l over the corresponding near-surface $t_{90}^{l=1,i,j}$ ($l = 1$ cm), these values are similar across all latitudes and times of year. For example, using the representative cases of June 21st and December 22nd at 40°S (Figure 3(b)), the curves of the ratio of $t_{90}^{l,i,j}$ to near-surface $t_{90}^{l=1,i,j}$ are similar despite much faster near-surface $t_{90}^{l=1,i,j}$ on December 22nd than June 21st. At any latitude or time of the year analyzed in this study, over 20 cm of well-mixed depth, we estimated $t_{90}^{l,i,j}$ to be between 11.2 and 11.6 times greater than near-surface $t_{90}^{l=1,i,j}$ values; over 50 cm of well-mixed depth, we estimated $t_{90}^{l,i,j}$ to be between 27.9 and 28.9 times greater than near-surface $t_{90}^{l=1,i,j}$ values.

In the present work, the diffuse attenuation coefficient, $K_{d,\lambda}$ was modeled using the DOC content of the wastewater sample used as an experimental matrix in this study. Although we made this assumption, there are differences in DOM concentration and composition among environmental waters that could result in near-surface decay rate constants that differ from the values predicted in this study.

Implications for WBE

The focus of this study was on sunlight-mediated decay of the SARS-CoV-2 N1 RNA target that is often used for wastewater surveillance of COVID-19, in PBS and sterile wastewater. While there was minimal decay observed in PBS, we observed

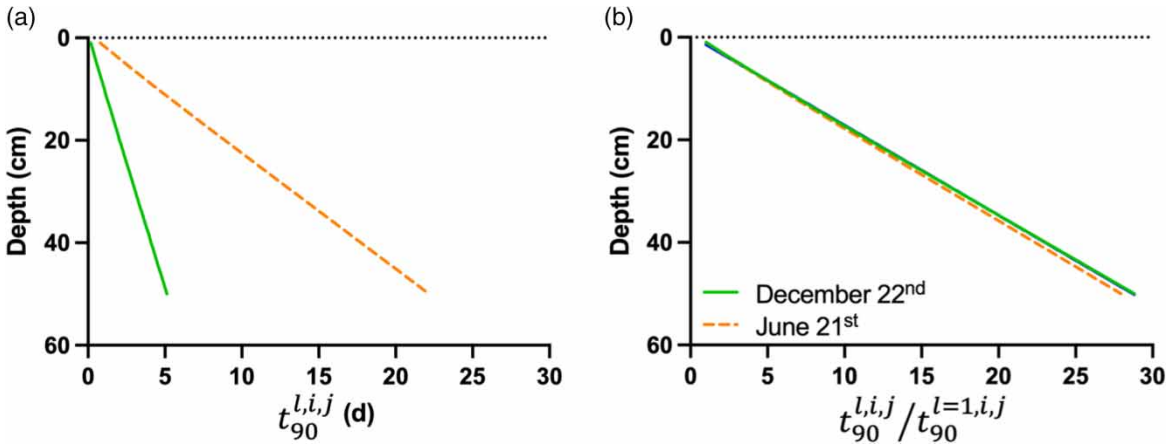

Figure 3 | (a) Predicted times required to reach 90% decay of the SARS-CoV-2 N1 gene target ($t_{90}^{l,i,j}$) over well-mixed depths up to 50 cm, for the representative cases of June 21st and December 22nd, at latitude of 40°S. (b) Predicted ratio of $t_{90}^{l,i,j}$ over well-mixed depth l to near-surface $t_{90}^{l=1,i,j}$ ($l = 1$ cm) for the N1 gene target for the representative cases of June 21st and December 22nd, at latitude of 40°S.

significant decay of the SARS-CoV-2 N1 gene target in sterile wastewater at shallow depths during laboratory experiments with exposure to simulated sunlight.

However, when accounting for environmental factors, including variations in sunlight irradiance across different latitudes at different times of the year and light attenuation in the water column, the impact of sunlight-mediated decay mechanisms on RNA persistence is likely minimal. For example, $t_{90}^{l,i,j}$ estimated over a well-mixed water depth of 10 cm and a latitude of 40°S are 4.5 and 1.1 d for June 21st and December 22nd, respectively; over a 50 cm well-mixed water depth these values are estimated to be 22.2 and 5.1 d for June 21st and December 22nd, respectively.

The predicted $t_{90}^{l,i,j}$ presented in this paper do not include additional RNA degradation and removal mechanisms that might occur in non-sterilized wastewater or environmental waters and affect the apparent decay kinetics of the N1 target – such as predation, enzymatic degradation, or adsorption to solids (Ye *et al.* 2016; Graham *et al.* 2021). Ahmed *et al.* determined t_{90} of the N1 gene target in untreated wastewater to be 27.8 $\pm$ 4.45, 20.4 $\pm$ 2.13, 12.6 $\pm$ 0.59, and 8.04 $\pm$ 0.23 d at temperatures of 4°, 15°, 25°, and 37 °C, respectively, under dark conditions – in which sunlight-independent processes (including biological and enzymatic activity) may be present and contribute to RNA decay. Given these results from Ahmed *et al.* and the finding herein that there is minimal sunlight-mediated decay of the N1 gene target in water columns with depths greater than a few centimeters, the N1 gene target is likely to be persistent in environmental waters. Therefore, in the case of WBE programs targeting surface waters, the environmental decay of the N1 gene target is not likely to confound results through underestimation of the concentration of the RT-qPCR target.

ACKNOWLEDGEMENTS

The authors thank Dr. Catherine Hoar for assistance in wastewater sampling.

FUNDING

F. B. D. was supported by the United States National Science Foundation, through a Graduate Research Fellowship and grant CBET-1846692 (made to A. I. S.).

DATA AVAILABILITY STATEMENT

All relevant data are included in the paper or its Supplementary Information.

CONFLICT OF INTEREST

The authors declare there is no conflict.

REFERENCES

Ahmed, W., Bertsch, P. M., Bibby, K., Haramoto, E., Hewitt, J., Huygens, F., Gyawali, P., Korajkic, A., Riddell, S., Sherchan, S. P., Simpson, S. L., Sirikanchana, K., Symonds, E. M., Verhagen, R., Vasan, S. S., Kitajima, M. & Bivins, A. 2020 Decay of SARS-CoV-2 and surrogate murine hepatitis virus RNA in untreated wastewater to inform application in wastewater-based epidemiology. *Environmental Research* **191**, 110092. https://doi.org/10.1016/j.envres.2020.110092.

Aloia, R. C., Jensen, F. C., Curtain, C. C., Mobley, P. W. & Gordon, L. M. 1988 Lipid composition and fluidity of the human immunodeficiency virus. *PNAS* **85**, 900–904. https://doi.org/10.1073/pnas.85.3.900.

Apell, J. N. & McNeill, K. 2019 Updated and validated solar irradiance reference spectra for estimating environmental photodegradation rates. *Environmental Science: Processes & Impacts* **21**, 427–437. https://doi.org/10.1039/C8EM00478A.

Appiani, E. & McNeill, K. 2015 Photochemical production of singlet oxygen from particulate organic matter. *Environmental Science & Technology* **49**, 3514–3522. https://doi.org/10.1021/es505712e.

Appiani, E., Ossola, R., Latch, D. E., Erickson, P. R. & McNeill, K. 2017 Aqueous singlet oxygen reaction kinetics of furfuryl alcohol: effect of temperature, pH, and salt content. *Environmental Science: Processes & Impacts* **19**, 507–516. https://doi.org/10.1039/C6EM00646A.

Bivins, A., North, D., Ahmad, A., Ahmed, W., Alm, E., Been, F., Bhattacharya, P., Bijlsma, L., Boehm, A. B., Brown, J., Buttiglieri, G., Calabro, V., Carducci, A., Castiglioni, S., Cetecioglu Gurol, Z., Chakraborty, S., Costa, F., Curcio, S., de los Reyes, F. L., Delgado Vela, J., Farkas, K., Fernandez-Casi, X., Gerba, C., Gerrity, D., Girones, R., Gonzalez, R., Haramoto, E., Harris, A., Holden, P. A., Islam, M. T., Jones, D. L., Kasprzyk-Hordern, B., Kitajima, M., Kotlarz, N., Kumar, M., Kuroda, K., La Rosa, G., Malpei, F., Mautus, M., McLellan, S. L., Medema, G., Meschke, J. S., Mueller, J., Newton, R. J., Nilsson, D., Noble, R. T., van Nuijs, A., Peccia, J., Perkins, T. A., Pickering, A. J., Rose, J., Sanchez, G., Smith, A., Stadler, L., Stauber, C., Thomas, K., van der Voorn, T., Wigginton, K., Zhu, K. & Bibby, K. 2020 Wastewater-based epidemiology: global collaborative to maximize contributions in the fight against COVID-19. *Environmental Science & Technology* **54**, 7754–7757. https://doi.org/10.1021/acs.est.0c02388

Cadet, J. & Teoule, R. 1978 Comparative study of oxidation of nucleic acid components by hydroxyl radicals, singlet oxygen and superoxide anion radicals. *Photochemistry and Photobiology* **28**, 661–665. https://doi.org/10.1111/j.1751-1097.1978.tb06991.x.

Calabria de Araujo, J., Gavazza, S., Leao, T. L., Florencio, L., da Silva, H. P., Albuquerque, J. d. O., de Lira Borges, M. A., de Oliveira Alves, R. B., Rodrigues, R. H. A. & dos Santos, E. B. 2020 SARS-CoV-2 sewage surveillance in low-income countries: potential and challenges. *Journal of Water and Health* **19**, 1–19. https://doi.org/10.2166/wh.2020.168.

Cooper, W. J., Zika, R. G., Petasne, R. G. & Fischer, A. M. 1988 Sunlight-induced photochemistry of humic substances in natural waters: major reactive species. In: *Aquatic Humic Substances, Advances in Chemistry*. American Chemical Society, pp. 333–362. https://doi.org/10.1021/ba-1988-0219.ch022.

Davies, M. J. 2003 Singlet oxygen-mediated damage to proteins and its consequences. *Biochemical and Biophysical Research Communications* **305**, 761–770. https://doi.org/10.1016/S0006-291X(03)00817-9.

Davies, M. J. & Truscott, R. J. W. 2001 Photo-oxidation of proteins and its role in cataractogenesis. *Journal of Photochemistry and Photobiology B: Biology, Consequences of Exposure to Sunlight: Elements to Assess Protection* **63**, 114–125. https://doi.org/10.1016/S1011-1344(01)00208-1.

Douki, T. 2006 Low ionic strength reduces cytosine photoreactivity in UVC-irradiated isolated DNA. *Photochemical & Photobiological Sciences* **5**, 1045–1051. https://doi.org/10.1039/B604517K.

Douki, T. & Cadet, J. 2001 Individual determination of the yield of the main UV-induced dimeric pyrimidine photoproducts in DNA suggests a high mutagenicity of CC photolesions. *Biochemistry* **40**, 2495–2501. https://doi.org/10.1021/bi0022543.

Dunn, F. B. & Silverman, A. I. 2021 Sunlight photolysis of extracellular and intracellular antibiotic resistance genes *tetA* and *sul2* in photosensitizer-free water. *Environmental Science & Technology* **55**, 11019–11028. https://doi.org/10.1021/acs.est.1c00732.

Erickson, P. R., Moor, K. J., Werner, J. J., Latch, D. E., Arnold, W. A. & McNeill, K. 2018 Singlet oxygen phosphorescence as a probe for triplet-state dissolved organic matter reactivity. *Environmental Science & Technology* **52**, 9170–9178. https://doi.org/10.1021/acs.est.8b02379.

Fisher, G. J. & Johns, H. E. 1976 Pyrimidine photohydrates. In: *Photochemistry and Photobiology of Nucleic Acids* (Wang, S.Y., ed.). Academic Press, New York, pp. 169–224.

Forootan, A., Sjöback, R., Björkman, J., Sjögreen, B., Linz, L. & Kubista, M. 2017 Methods to determine limit of detection and limit of quantification in quantitative real-time PCR (qPCR). *Biomolecular Detection and Quantification* **12**, 1–6. https://doi.org/10.1016/j.bdq.2017.04.001.

Gordon, M. P., Huang, C. & Hurter, J., 1976 7 - Photochemistry and photobiology of ribonucleic acids, ribonucleoproteins, and RNA viruses. In: *Photochemistry and Photobiology of Nucleic Acids* (Wang, S. Y., ed.). Academic Press, pp. 265–308. https://doi.org/10.1016/B978-0-12-734602-1.50013-7.

Görner, H. 1994 New trends in photobiology: photochemistry of DNA and related biomolecules: quantum yields and consequences of photoionization. *Journal of Photochemistry and Photobiology B: Biology* **26**, 117–139. https://doi.org/10.1016/1011-1344(94)07068-7.

Graham, K. E., Loeb, S. K., Wolfe, M. K., Catoe, D., Sinnott-Armstrong, N., Kim, S., Yamahara, K. M., Sassoubre, L. M., Mendoza Grijalva, L. M., Roldan-Hernandez, L., Langenfeld, K., Wigginton, K. R. & Boehm, A. B. 2021 SARS-CoV-2 RNA in wastewater settled solids is associated with COVID-19 cases in a large urban sewershed. *Environmental Science & Technology* **55**, 488–498. https://doi.org/10.1021/acs.est.0c06191.

Gröner, A., Broumis, C., Fang, R., Nowak, T., Popp, B., Schäfer, W. & Roth, N. J. 2018 Effective inactivation of a wide range of viruses by pasteurization. *Transfusion* **58**, 41–51. https://doi.org/10.1111/trf.14390.

Gueymard, C. A. 2005 Interdisciplinary applications of a versatile spectral solar irradiance model: a review. *Energy, Measurement and Modelling of Solar Radiation and Daylight - Challenges for the 21st Century* **30**, 1551–1576. https://doi.org/10.1016/j.energy.2004.04.032.

Hillary, L. S., Farkas, K., Maher, K. H., Lucaci, A., Thorpe, J., Distaso, M. A., Gaze, W. H., Paterson, S., Burke, T., Connor, T. R., McDonald, J. E., Malham, S. K. & Jones, D. L. 2021 Monitoring SARS-CoV-2 in municipal wastewater to evaluate the success of lockdown measures for controlling COVID-19 in the UK. *Water Research* **200**, 117214. https://doi.org/10.1016/j.watres.2021.117214.

Ho, J., Seidel, M., Niessner, R., Eggers, J. & Tiehm, A. 2016 Long amplicon (LA)-qPCR for the discrimination of infectious and noninfectious phix174 bacteriophages after UV inactivation. *Water Research* **103**, 141–148. https://doi.org/10.1016/j.watres.2016.07.032.

Hoar, C., Chauvin, F., Clare, A., McGibbon, H., Castro, E., Patinella, S., Katehis, D., Dennehy, J. J., Trujillo, M., Smyth, D. S. & Silverman, A. I. 2022 Monitoring SARS-CoV-2 in wastewater during New York City's second wave of COVID-19: sewershed-level trends and relationships to publicly available clinical testing data. *Environmental Science: Water Research & Technology* **8**, 1021–1035. https://doi.org/10.1039/D1EW00747E.

Jagger, J. 1985 *Solar-UV Actions on Living Cells*. Praeger, New York.

Kazama, S., Miura, T., Masago, Y., Konta, Y., Tohma, K., Manaka, T., Liu, X., Nakayama, D., Tanno, T., Saito, M., Oshitani, H. & Omura, T. 2017 Environmental surveillance of norovirus genogroups I and II for sensitive detection of epidemic variants. *Applied and Environmental Microbiology*. https://doi.org/10.1128/AEM.03406-16.

Latch, D. E. & McNeill, K. 2006 Microheterogeneity of singlet oxygen distributions in irradiated humic acid solutions. *Science* **311**, 1743–1747. https://doi.org/10.1126/science.1121636.

Lee, W. L., Imakaev, M., Armas, F., McElroy, K. A., Gu, X., Duvallet, C., Chandra, F., Chen, H., Leifels, M., Mendola, S., Floyd-O'Sullivan, R., Powell, M. M., Wilson, S. T., Berge, K. L. J., Lim, C. Y. J., Wu, F., Xiao, A., Moniz, K., Ghaeli, N., Matus, M., Thompson, J. & Alm, E. J. 2021 Quantitative SARS-CoV-2 alpha variant B.1.1.7 tracking in wastewater by allele-specific RT-qPCR. *Environmental Science & Technology Letters* **8**, 675–682. https://doi.org/10.1021/acs.estlett.1c00375.

Lu, X., Wang, L., Sakthivel, S. K., Whitaker, B., Murray, J., Kamili, S., Lynch, B., Malapati, L., Burke, S. A., Harcourt, J., Tamin, A., Thornburg, N. J., Villanueva, J. M. & Lindstrom, S. 2020 US CDC real-time reverse transcription PCR panel for detection of severe acute respiratory syndrome coronavirus 2. *Emerging Infectious Diseases* **26**, 1654–1665. https://doi.org/10.3201/eid2608.201246.

Lundy, L., Fatta-Kassinos, D., Slobodnik, J., Karaolia, P., Cirka, L., Kreuzinger, N., Castiglioni, S., Bijlsma, L., Dulio, V., Deviller, G., Lai, F. Y., Alygizakis, N., Barneo, M., Baz-Lomba, J. A., Béen, F., Číchová, M., Conde-Pérez, K., Covaci, A., Donner, E., Ficek, A., Hassard, F., Hedström, A., Hernandez, F., Janská, V., Jellison, K., Hofman, J., Hill, K., Hong, P.-Y., Kasprzyk-Hordern, B., Kolarević, S., Krahulec, J., Lambropoulou, D., de Llanos, R., Mackuľak, T., Martinez-García, L., Martínez, F., Medema, G., Micsinai, A., Myrmel, M., Nasser, M., Niederstätter, H., Nozal, L., Oberacher, H., Očenášková, V., Ogorzaly, L., Papadopoulos, D., Peinado, B., Pitkänen, T., Poza, M., Rumbo-Feal, S., Sánchez, M.B., Székely, A.J., Soltysova, A., Thomaidis, N.S., Vallejo, J., van Nuijs, A., Ware, V. & Viklander, M. 2021 Making waves: collaboration in the time of SARS-CoV-2 – rapid development of an international co-operation and wastewater surveillance database to support public health decision-making. *Water Research* **199**, 117167. https://doi.org/10.1016/j.watres.2021.117167.

Manor, Y., Handsher, R., Halmut, T., Neuman, M., Bobrov, A., Rudich, H., Vonsover, A., Shulman, L., Kew, O. & Mendelson, E. 1999 Detection of poliovirus circulation by environmental surveillance in the absence of clinical cases in Israel and the Palestinian authority. *Journal of Clinical Microbiology*. https://doi.org/10.1128/JCM.37.6.1670-1675.1999.

Miller, R. L. & Plageman, P. G. W. 1974 Effect of ultraviolet light on mengovirus: formation of uracil dimers, instability and degradation of capsid, and covalent linkage of protein to viral RNA. *Journal of Virology* **13**, 729–739. https://doi.org/10.1128/jvi.13.3.729-739.1974.

Nelson, K. L., Boehm, A. B., Davies-Colley, R. J., Dodd, M. C., Kohn, T., Linden, K. G., Liu, Y., Maraccini, P. A., McNeill, K., Mitch, W. A., Nguyen, T. H., Parker, K. M., Rodriguez, R. A., Sassoubre, L. M., Silverman, A. I., Wigginton, K. R. & Zepp, R. G. 2018 Sunlight-mediated inactivation of health-relevant microorganisms in water: a review of mechanisms and modeling approaches. *Environmental Science: Processes Impacts* **20**, 1089–1122. https://doi.org/10.1039/C8EM00047F.

Park, S., Lee, C.-W., Park, D.-I., Woo, H.-Y., Cheong, H. S., Shin, H. C., Ahn, K., Kwon, M.-J. & Joo, E.-J. 2021 Detection of SARS-CoV-2 in fecal samples from patients with asymptomatic and mild COVID-19 in Korea. *Clinical Gastroenterology and Hepatology* **19**, 1387–1394.e2. https://doi.org/10.1016/j.cgh.2020.06.005.

Partanen, S. B., Erickson, P. R., Latch, D. E., Moor, K. J. & McNeill, K. 2020 Dissolved organic matter singlet oxygen quantum yields: evaluation using time-resolved singlet oxygen phosphorescence. *Environmental Science & Technology* **54**, 3316–3324. https://doi.org/10.1021/acs.est.9b07246.

Partanen, S. B., Apell, J. N., Lin, J. & McNeill, K. 2021 Factors affecting the mixed-layer concentrations of singlet oxygen in sunlit lakes. *Environmental Science: Processes & Impacts*. https://doi.org/10.1039/D1EM00062D.

Pfaender, S., Brinkmann, J., Todt, D., Riebesehl, N., Steinmann, J., Steinmann, J., Pietschmann, T. & Steinmann, E. 2015 Mechanisms of methods for hepatitis C virus inactivation. *Applied and Environmental Microbiology* **81**, 1616–1621. https://doi.org/10.1128/AEM.03580-14.

Qiao, Z. & Wigginton, K. R. 2016 Direct and indirect photochemical reactions in viral RNA measured with RT-qPCR and mass spectrometry. *Environmental Science & Technology* **50**, 13371–13379. https://doi.org/10.1021/acs.est.6b04281.

Randazzo, W., Truchado, P., Cuevas-Ferrando, E., Simón, P., Allende, A. & Sánchez, G. 2020 SARS-CoV-2 RNA in wastewater anticipated COVID-19 occurrence in a low prevalence area. *Water Research* **181**, 115942. https://doi.org/10.1016/j.watres.2020.115942.

Ravanat, J.-L., Douki, T. & Cadet, J. 2001 Direct and indirect effects of UV radiation on DNA and its components. *Journal of Photochemistry and Photobiology B: Biology, Consequences of Exposure to Sunlight: Elements to Assess Protection* **63**, 88–102. https://doi.org/10.1016/S1011-1344(01)00206-8.

Richter, Ł., Księżarczyk, K., Paszkowska, K., Janczuk-Richter, M., Niedziółka-Jönsson, J., Gapiński, J., Łoś, M., Hołyst, R. & Paczesny, J. 2021 Adsorption of bacteriophages on polypropylene labware affects the reproducibility of phage research. *Science Reports* **11**, 7387. https://doi.org/10.1038/s41598-021-86571-x.

Rios, G., Lacoux, C., Leclercq, V., Diamant, A., Lebrigand, K., Lazuka, A., Soyeux, E., Lacroix, S., Fassy, J., Couesnon, A., Thiery, R., Mari, B., Pradier, C., Waldmann, R. & Barbry, P. 2021 Monitoring SARS-CoV-2 variants alterations in nice neighborhoods by wastewater nanopore sequencing. *The Lancet Regional Health – Europe* **10**, 100202. https://doi.org/10.1016/j.lanepe.2021.100202.

Rocha, A. Y., Verbyla, M. E., Sant, K. E. & Mladenov, N. 2022 Detection, quantification, and simplified wastewater surveillance model of SARS-CoV-2 RNA in the Tijuana River. *ACS EST Water*. https://doi.org/10.1021/acsestwater.2c00062.

Sagripanti, J.-L. & Lytle, C. D. 2020 Estimated inactivation of coronaviruses by solar radiation with special reference to COVID-19. *Photochemistry and Photobiology* **96**, 731–737. https://doi.org/10.1111/php.13293.

Silverman, A. I., Tay, N. & Machairas, N. 2019 Comparison of biological weighting functions used to model endogenous sunlight inactivation rates of MS2 coliphage. *Water Research* **151**, 439–446. https://doi.org/10.1016/j.watres.2018.12.015.

Tang, A., Tong, Z., Wang, H., Dai, Y., Li, K., Liu, J., Wu, W., Yuan, C., Yu, M., Li, P. & Yan, J. 2020 Detection of novel coronavirus by RT-PCR in stool specimen from asymptomatic child, China. *Emerging Infectious Diseases Journal – CDC* **26**. https://doi.org/10.3201/eid2606.200301.

Wigginton, K. R., Pecson, B. M., Sigstam, T., Bosshard, F. & Kohn, T. 2012 Virus inactivation mechanisms: impact of disinfectants on virus function and structural integrity. *Environmental Science & Technology* **46**, 12069–12078. https://doi.org/10.1021/es3029473.

Williams, G. J. 2009 *The Effect of Loading Rate on Tertiary Wastewater Filtration*. *PhD Dissertation*, University of California, Berkeley, CA.

Wurtmann, E. J. & Wolin, S. L. 2009 RNA under attack: cellular handling of RNA damage. *Critical Reviews in Biochemistry and Molecular Biology* **44**, 34–49. https://doi.org/10.1080/10409230802594043.

Ye, Y., Ellenberg, R. M., Graham, K. E. & Wigginton, K. R. 2016 Survivability, partitioning, and recovery of enveloped viruses in untreated municipal wastewater. *Environmental Science & Technology* **50**, 5077–5085. https://doi.org/10.1021/acs.est.6b00876.

Zhang, X., Li, J., Fan, W.-Y., Yao, M.-C., Yuan, L. & Sheng, G.-P. 2019 Enhanced photodegradation of extracellular antibiotic resistance genes by dissolved organic matter photosensitization. *Environmental Science & Technology* **53**, 10732–10740. https://doi.org/10.1021/acs.est.9b03096.

Zhang, T., Cheng, F., Yang, H., Zhu, B., Li, C., Zhang, Y., Qu, J. & Peijnenburg, W. J. G. M. 2022 Photochemical degradation pathways of cell-free antibiotic resistance genes in water under simulated sunlight irradiation: experimental and quantum chemical studies. *Chemosphere* **302**, 134879. https://doi.org/10.1016/j.chemosphere.2022.134879.

First received 24 April 2023; accepted in revised form 11 August 2023. Available online 23 August 2023